IEEE Access
Multidisciplinary ⋮ Rapid Review ⋮ Open Access Journal

Received 16 July 2024, accepted 30 July 2024, date of publication 5 August 2024, date of current version 14 August 2024.

Digital Object Identifier 10.1109/ACCESS.2024.3438286

RESEARCH ARTICLE

Analytical Frequency Security Indicators for Two-Region Interconnected Power Systems

QIANG ZHANG[1], XINWEI LI[1], GUORONG LAN[2], (Graduate Student Member, IEEE), XIANGXU WANG[2], (Graduate Student Member, IEEE), JIAKAI SHEN[3], HUI ZENG[1,2], PENG YUAN[1], XIAOHENG ZHANG[1], AND WEIDONG LI[2], (Member, IEEE)

[1]State Grid Liaoning Electric Power Research Institute, Shenyang 110006, China
[2]School of Electrical Engineering, Dalian University of Technology, Dalian 116024, China
[3]China Electric Power Research Institute, Beijing 100192, China

Corresponding author: Weidong Li (wdli@dlut.edu.cn)

This work was supported in part by the Science and Technology Project of State Grid under Grant 2023YF-76.

ABSTRACT Frequency spatial distribution characteristics of interconnected power systems are highlighted, resulting in significant regional frequency differences and inter-region tie-line power fluctuations, posing a threat to frequency security operation. For two-region interconnected power systems, analytical expressions for regional frequency and inter-regional tie-line power are derived based on the low-order frequency response model. By dividing the fast-varying part and the slow-varying part of the above analytical expressions, analytical frequency security indicators including nadir value, quasi-steady-state value, maximum rate value of regional frequency, and peak value, quasi-steady-state value of inter-regional tie-line power are derived. By dividing the fast-varying part and slow-varying part of the aforementioned analytical expressions, we further derived analytical frequency security indicators, including nadir value, quasi-steady-state value, maximum rate value of regional frequency, and peak value, quasi-steady-state value of inter-area tie-line power. Through case studies based on the IEEE 2-region 4-machine system, the results indicate that the obtained analytical frequency security indicators can accurately describe the frequency dynamics following a major disturbance for two-region interconnected power systems.

INDEX TERMS Frequency security indicators, interconnected power systems, frequency nadir, inter-regional tie-line power, analytical method.

I. INTRODUCTION

As the new power systems evolve, the individual generator capacity, renewable generation supply capability, and UHV inter-regional transmission capability have increased, leading to a considerable increase in the power deficit caused by single component failures [1]. On the other hand, as the proportion of low inertia renewable energy sources and power electronic devices increases, the system inertia and Primary Frequency Regulation (PFR) capacity gradually decrease [2]. Under the dual effects of increased disturbance risk and decreased disturbance resilience, the frequency stability situation of interconnected power systems becomes increasingly severe [3].

Meanwhile, influenced by the construction of large-scale renewable generation bases, the distribution of inertia and PFR capacity in the system becomes more uneven [4]. Additionally, the expansion of system-scale results in increased electrical distances between regions, weakening their connections further [5]. Therefore, The frequency spatial distribution characteristics following disturbances of interconnected power systems become more significant [6], and the frequency dynamics analysis method should be up-to-date.

Currently, there are three main methods for frequency dynamics analysis: data-driven methods, simulation methods, and analytical methods. Data-driven methods provide a

The associate editor coordinating the review of this manuscript and approving it for publication was Lei Chen.

more comprehensive and accurate analysis of the frequency dynamics of complex systems [7]. However, data-driven methods require a large amount of high-quality data for training and validation, and the performance of the models may significantly degrade if the data is insufficient or of low quality [8]. Simulation methods can accurately simulate the physical behavior and dynamic characteristics of power systems, considering detailed models of various devices and components. They also allow control and setting of various conditions and events in the simulation for testing and analysis of different scenarios. The downside is that high-precision simulations require substantial computational resources and time, especially for the dynamic simulation of large-scale power systems, where the cost of computational resources and time increases significantly with the scale and precision of the simulation [9]. Analytical methods can derive explicit functional relationships of frequency dynamics over time, enabling direct calculation of frequency values at any given moment without iteration [10]. Due to their clear form and high computational efficiency, analytical methods are widely used in various scenarios. For instance, in fast calculation scenarios, analytical methods are very suitable for online computation [11]. Additionally, in scenarios requiring large-scale computations such as unit testing, analytical methods perform excellently [12]. In theoretical analysis scenarios, analytical methods are often used for parameter sensitivity analysis, showcasing their unique advantages [13]. In interconnected power systems, Analytical Frequency Security Indicators (AFSIs) usually include the nadir value, quasi-steady-state value, and maximum rate value during the dynamic frequency process [14]. These indicators provide a basis for unit commitment before incidents [15], frequency stability control during incidents [16], and performance evaluation after incidents [17], making them one of the research hotspots in recent years.

Since the frequency spatial distribution characteristics in isolated power systems are not significant, most of the existing frequency security analysis indicators are derived based on the assumption of average frequency. Reference [10] derived analytical expressions for the nadir value, quasi-steady-state value, and maximum rate value of system frequency based on the analytical expressions of a low-order system frequency response model. Reference [18] derived a low-order average system frequency model based on a first-order inertia feedback regulator. References [19] and [20] derived the analytical expression of the nadir value through frequency feedback loops and frequency deviation approximation, providing references for frequency dynamics analysis.

Unlike isolated power systems, the frequency dynamics of interconnected power systems exhibit significant spatial distribution characteristics after disturbances [21]. Specifically, the AFSIs of each region differ significantly from the center of inertia, regions mutually influence each other, and the inter-regional tie-line power (ITP) fluctuates greatly [22], [23]. Most existing studies focus on isolated power systems and ignore the frequency spatial distribution characteristics, rendering the derived frequency security analysis indicators unsuitable for interconnected power systems.

For interconnected power systems, [24] derived several Taylor series for AFSIs in a two-area system. However, to ensure accuracy, these Taylor series need to retain nearly a hundred terms, which limits their application. References [25] and [26] proposed low-order frequency response models for two-area and three-area power systems and derived analytical expressions for Regional Frequency (RF). Although analytical expressions for frequency dynamics, consisting of central frequency and inter-machine oscillation frequency, have been obtained, these functions exhibit multi-peak and non-monotonic characteristics, making it impossible to quickly solve AFSIs using conventional methods. Additionally, they do not provide analytical methods for ITP. Reference [27] considered the steady-state value of ITP but ignored dynamic characteristics and did not consider its peak value. Reference [28] proposed a linearized model for ITP fluctuations between two main areas and derived the analytical expression for the peak value. Reference [29] further calculated the peak value of ITP following faults such as DC blocking. However, these studies did not consider the grid connection capacity of generators. Therefore, there is still a lack of accurate AFSIs that can describe RF and ITP.

This paper focuses on the interconnected power systems of two regions, contributing primarily in the following two aspects:

1) Simplification of the two region interconnected power system into a low-order two-machine frequency response models based on structural characteristics, and derivation of analytical expressions for RF and ITP.
2) By dividing the analytical expressions into fast-varying part and the slow-varying part, deriving AFSIs including nadir value, quasi-steady-state value, maximum rate value of RF, and peak value, quasi-steady-state value of ITP.

The rest of the paper is organized as follows. Section II proposes the low-order frequency response model for the two-region interconnected power system and derive its analytical expression. Section III divides the fast-varying part and the slow-varying of the obtained analytical expressions and derives the AFSIs for the RF and the ITP. Section IV conducts case studies and provides simulation results. Section V concludes the paper.

II. MODELING AND ANALYTICAL DERIVATION

A. FREQUENCY RESPONSE MODEL

For the two-region power system, aggregating each region into an equivalent generator [20], simplifying the network structure based on DC power flow [24], and reducing the model order complexity with the low-order governor model [30], a low-order frequency response model can be developed, as shown in Fig. 1.

where, x_{I} is the corresponding x of the equivalent generator for the Region-I, x_{II} is the corresponding x of the

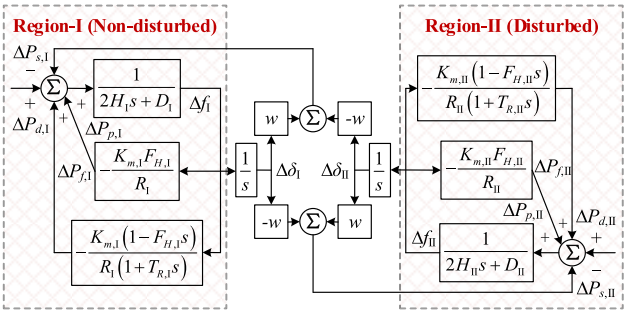

FIGURE 1. The low-order frequency response model for the two-region power system (assuming Region-II is the disturbed region).

equivalent generator for the Region-II, H is the inertia time constant, D is the damping coefficient,K_m is the mechanical power gain coefficient,F_H is the high-pressure turbine power coefficient, R is the governor regulation coefficient,T_R is the reheating time constant, P_m is the mechanical power, δ is the rotor angle, f is the frequency, ΔP_d is the disturbance power, ΔP_s is the inter-region oscillation power, ΔP_p is the proportional feedback power, ΔP_f is the first-order inertial feedback power, Δ is the deviation symbol, s is the complex variable symbol in Laplace transform,w is the equivalent branch admittance:

$$w = \omega_0 B_s \tag{1}$$

where, ω_0 is the rated angular velocity, B_s is the branch admittance.

With the development of renewable energy sources, their PFR capacity should be considered. Currently, the PFR function modification of renewable energy is mainly to add frequency control loops (e.g., virtual inertia control and virtual droop control) that simulate the PFR characteristics of conventional generators in its active power control system. Since the added PFR loops have similar structures, they can be equivalently aggregated with conventional generators [31].

According to [13], the equivalent parameters of each region can be aggregated from the system network and the parameters of all generators in the region. Next, we will take Region-I as an example and provide the calculation method for each equivalent parameter. The same procedure applies to Region-II.

Let S_B be the base capacity of the generator and line parameters, then $K_{m,\mathrm{I},i}$ for each generator within the region can be expressed as

$$K_{m,\mathrm{I},i} = \frac{\Delta P_{\max,i}}{S_B}, \quad i \in \mathbf{V}_\mathrm{I} \tag{2}$$

where, i is the index of all generators in the system, $\boldsymbol{V}_\mathrm{I}$ is the set of generators in Region-I, $\Delta P_{\max,i}$ is the rated power of the i-th generator.

Let $X = \{H, D\}$, $Y = \{F_H, T_R\}$, then X_I and Y_I can be expressed as

$$X_\mathrm{I} = \sum_{i \in V_\mathrm{I}} K_{m,\mathrm{I},i} X_{\mathrm{I},i}, \quad Y_\mathrm{I} = \frac{\sum\limits_{i \in \mathbf{V}_\mathrm{I}} Y_{\mathrm{I},i} K_{m,\mathrm{I},i} R_{\mathrm{I},i}^{-1}}{\sum\limits_{i \in \mathbf{V}_\mathrm{I}} K_{m,\mathrm{I},i} R_{\mathrm{I},i}^{-1}} \tag{3}$$

where

$$R_\mathrm{I}^{-1} = \frac{\sum\limits_{i \in V_\mathrm{I}} K_{m,\mathrm{I},i} R_{\mathrm{I},i}^{-1}}{K_{m,\mathrm{I}}}, \quad K_{m,\mathrm{I}} = \sum_{i \in V_\mathrm{I}} K_{m,\mathrm{I},i} \tag{4}$$

The electromagnetic power variation of the equivalent generator for Region-I is the difference between $\Delta P_{d,\mathrm{I}}$ and $\Delta P_{s,\mathrm{I}}$. Meanwhile, the ITP variation represents the supporting power from the non-disturbed region to the disturbed region, which is equal to the electromagnetic power variation of the equivalent generator for the non-disturbed region. In this paper, we assume that Region-II is the disturbed region and region-I is the non-disturbed region. Therefore, the ITP ΔP_t can be expressed as

$$\Delta P_t = \Delta P_{s,\mathrm{I}} - \Delta P_{d,\mathrm{I}} = w\left(\Delta\delta_\mathrm{I} - \Delta\delta_\mathrm{II}\right) - \sum_{i \in V_\mathrm{I}} \Delta P_{d,\mathrm{I},i} \tag{5}$$

B. ANALYTICAL EXPRESSIONS FOR THE RF

Based on the modal analysis method proposed in [24], the mathematic equation of the model shown in Fig. 1 can be transformed into a second-order two-degree-of-freedom forced vibration equation with y_I and y_II as the primary modal coordinates, as shown below:

$$2H_{\mathrm{sys}}\ddot{y}_\mathrm{I} + D_{\mathrm{eq,sys}}\dot{y}_\mathrm{I} = \omega_0\left(\Delta P_{d,\mathrm{sys}} + \Delta P_{f,\mathrm{sys}} - \chi_3\dot{y}_\mathrm{II}\right) \tag{6}$$

$$\begin{aligned} &4H_{\mathrm{sys}}H_\mathrm{I}H_\mathrm{II}\ddot{y}_\mathrm{II} + 2\left(H_\mathrm{I}^2 D_{eq,\mathrm{II}} + H_\mathrm{II}^2 D_{eq,\mathrm{I}}\right)\dot{y}_\mathrm{II} \\ &\quad + 2wH_{\mathrm{sys}}^2 y_\mathrm{II} = \omega_0\left(\chi_1 + \chi_2 - \chi_3\dot{y}_\mathrm{I}\right) \end{aligned} \tag{7}$$

where, x_{sys} is the corresponding x of the low-order system frequency response model proposed in [10] and can be calculated by the equivalent aggregation method proposed in [13], D_{eq} is the the equivalent damping coefficient, χ_1, χ_2, and χ_3 are three input powers:

$$\begin{cases} D_{eq} = D + K_m F_H R^{-1} \\ \chi_1 = 2H_\mathrm{I}\Delta P_{d,\mathrm{II}} - 2H_\mathrm{II}\Delta P_{d,\mathrm{I}} \\ \chi_2 = 2H_\mathrm{I}\Delta P_{f,\mathrm{II}} - 2H_\mathrm{II}\Delta P_{f,\mathrm{I}} \\ \chi_3 = 2H_\mathrm{I}D_{eq,\mathrm{II}} - 2H_\mathrm{II}D_{eq,\mathrm{I}} \end{cases} \tag{8}$$

Therefore, the RF can be expressed as the product of the modal matrix $\boldsymbol{\Phi}$ and the primary modal coordinates:

$$\begin{bmatrix} \Delta f_\mathrm{I} \\ \Delta f_\mathrm{II} \end{bmatrix} = \begin{bmatrix} \Delta\dot{\delta}_\mathrm{I} \\ \Delta\dot{\delta}_\mathrm{II} \end{bmatrix} = \boldsymbol{\Phi}\dot{\boldsymbol{y}} = \begin{bmatrix} 1 & -2H_\mathrm{II} \\ 1 & 2H_\mathrm{I} \end{bmatrix} \begin{bmatrix} \dot{y}_\mathrm{I} \\ \dot{y}_\mathrm{II} \end{bmatrix} \tag{9}$$

Since $\chi_3\dot{y}_\mathrm{II}$ shows little effect on $\dot{y}_\mathrm{I}$ in (7), and $\chi_2 - \chi_3\dot{y}_\mathrm{I}$ shows little effect on $\dot{y}_\mathrm{II}$ in (8), they can be ignored to decouple $\dot{y}_\mathrm{I}$ and $\dot{y}_\mathrm{II}$ and solve for them separately:

$$\begin{cases} \dot{y}_\mathrm{I}(t) = \omega_0\alpha_1 e^{-\zeta_1\omega_{n,1}t}\sin\left(\omega_{r,1}t + \varphi\right) + \omega_0\beta \\ \dot{y}_\mathrm{II}(t) = \omega_0\alpha_2 e^{-\zeta_2\omega_{n,2}t}\sin\omega_{r,2}t \end{cases} \tag{10}$$

where

$$\begin{cases} \omega_{n,1} = \sqrt{\dfrac{D_{\text{sys}}R_{\text{sys}} + K_{m,\text{sys}}}{2H_{\text{sys}}R_{\text{sys}}T_{R,\text{sys}}}} \\ \zeta_1 = \omega_{n,1}\dfrac{2H_{\text{sys}}R_{\text{sys}} + \left(D_{\text{sys}}R_{\text{sys}} + K_{m,\text{sys}}F_{H,\text{sys}}\right)T_{R,\text{sys}}}{2\left(D_{\text{sys}}R_{\text{sys}} + K_{m,\text{sys}}\right)} \\ \omega_{r,1} = \omega_{n,1}\sqrt{1-\zeta_1^2} \\ \beta = \dfrac{R_{\text{sys}}\Delta P_{d,\text{sys}}}{D_{\text{sys}}R_{\text{sys}} + K_{m,\text{sys}}} \\ \alpha_1 = \beta\sqrt{\dfrac{1 - 2T_{R,\text{sys}}\zeta_1\omega_{n,1} + T_{R,\text{sys}}^2\omega_{n,1}^2}{1-\zeta_1^2}} \\ \varphi = \tan^{-1}\left(\dfrac{\sqrt{1-\zeta_1^2}}{\zeta_1 - \omega_{n,1}T_{R,\text{sys}}}\right) \end{cases} \tag{11}$$

$$\begin{cases} \omega_{n,2} = \sqrt{\dfrac{w}{2H_{\text{I}}} + \dfrac{w}{2H_{\text{II}}}} \\ \zeta_2 = \omega_{n,2}\dfrac{H_{\text{I}}^2D_{eq,2} + H_{\text{II}}^2D_{eq,1}}{w\left(H_{\text{I}} + H_{\text{II}}\right)^2} \\ \omega_{r,2} = \omega_{n,2}\sqrt{1-\zeta_2^2} \\ \alpha_2 = \dfrac{H_{\text{I}}\Delta P_{d,\text{I}} - H_{\text{II}}\Delta P_{d,\text{II}}}{2H_{\text{I}}H_{\text{II}}\omega_{r,2}\left(H_{\text{I}} + H_{\text{II}}\right)} \end{cases} \tag{12}$$

Substitute (10) into (9), the analytical expressions for $\Delta f_{\text{I}}(t)$ and $\Delta f_{\text{II}}(t)$ can be expressed as

$$\begin{aligned} \Delta f_{\text{I}}(t) &= \alpha_1 e^{-\zeta_1\omega_{n,1}t}\sin\left(\omega_{r,1}t + \varphi\right) + \beta \\ &\quad - 2H_{\text{II}}\alpha_2 e^{-\zeta_2\omega_{n,2}t}\sin\omega_{r,2}t \end{aligned} \tag{13.a}$$

$$\begin{aligned} \Delta f_{\text{II}}(t) &= \alpha_1 e^{-\zeta_1\omega_{n,1}t}\sin\left(\omega_{r,1}t + \varphi\right) + \beta \\ &\quad + 2H_{\text{I}}\alpha_2 e^{-\zeta_2\omega_{n,2}t}\sin\omega_{r,2}t \end{aligned} \tag{13.b}$$

Taking the derivative of (13), the analytical expressions for the RoCoF can be obtain as

$$\begin{aligned} \Delta\dot{f}_{\text{I}}(t) &= \alpha_1\omega_{n,1}e^{-\zeta_1\omega_{n,1}t}\sin\left(\omega_{r,1}t + \varphi_1\right) \\ &\quad - 2H_{\text{II}}\alpha_2\omega_{n,2}e^{-\zeta_2\omega_{n,2}t}\sin\left(\omega_{r,2}t + \varphi_2\right) \end{aligned} \tag{14.a}$$

$$\begin{aligned} \Delta\dot{f}_{\text{II}}(t) &= \alpha_1\omega_{n,1}e^{-\zeta_1\omega_{n,1}t}\sin\left(\omega_{r,1}t + \varphi_1\right) \\ &\quad + 2H_{\text{I}}\alpha_2\omega_{n,2}e^{-\zeta_2\omega_{n,2}t}\sin\left(\omega_{r,2}t + \varphi_2\right) \end{aligned} \tag{14.b}$$

where

$$\begin{cases} \varphi_1 = \tan^{-1}\left(\dfrac{\omega_{r,1}T_{R,\text{sys}}}{1 - \zeta_1\omega_{n,1}T_{R,\text{sys}}}\right) \\ \varphi_2 = \tan^{-1}\left(-\dfrac{\sqrt{1-\zeta_2^2}}{\zeta_2}\right) \end{cases} \tag{15}$$

C. ANALYTICAL EXPRESSIONS FOR THE ITP

Combining (5) and (9), the relationship between $\Delta P_{s,\text{I}}$ and the primary modal coordinates can be obtained as

$$\begin{aligned} \Delta P_{s,\text{I}}(t) &= w\Delta\delta_{\text{I}}(t) - w\Delta\delta_{\text{II}}(t) \\ &= w\int \Delta f_{\text{I}}(t) - \Delta f_{\text{II}}(t)\,dt = -2wH_{\text{sys}}y_{\text{II}}(t) \end{aligned} \tag{16}$$

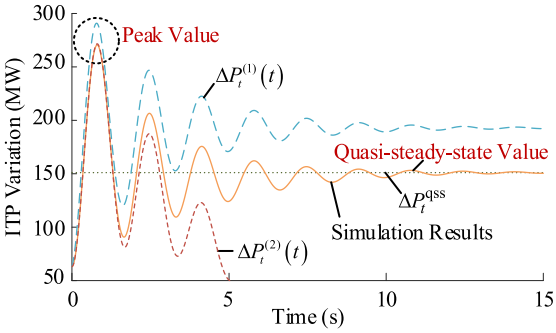

FIGURE 2. The Comparison of analytical and simulation results of the ITP variation.

Substituting (13) into (16), the simplified form of $\Delta P_{s,\text{I}}^{(1)}(t)$ can be obtained. by substituting $\Delta P_{s,\text{I}}^{(1)}(t)$ into (5), the simplified form of $\Delta P_t^{(1)}(t)$ can be derived. Comparing with the simulation results, it is observed that there are significant errors in both the peak value and the quasi-steady-state value, as shown in Fig. 2. Therefore, the $\Delta P_t^{(1)}(t)$ obtained from this method cannot accurately describe the ITP variation.

It is verified that these errors are caused by the neglect made in solving (10). These neglect terms have a small effect on the RF, but their integration has a significant effect on the ITP and should therefore be taken into account when derivating the analytical expressions for the ITP.

1) PEAK VALUE

The maximum value of the ITP occurs at the first swing peak of its oscillation. Within this time scale, the governor can be considered unresponsive and the RoCoF can be considered constant. Therefore, (7) can be simplified as

$$\ddot{y}_{\text{II}}(t) + 2\zeta_2\omega_{n,2}\dot{y}_{\text{II}}(t) + \omega_{n,2}^2 y_{\text{II}}(t) = \frac{2H_{\text{sys}}\chi_1 + \Delta P_{d,\text{sys}}\chi_3 t}{16H_{\text{sys}}^2H_{\text{I}}H_{\text{II}}} \tag{17}$$

Solving (17) and substituting it into (16) yields $\Delta P_{s,\text{I}}^{(2)}(t)$. Then substituting it into (5), $\Delta P_t^{(2)}(t)$ can be obtained as

$$\Delta P_t^{(2)}(t) = \rho_1 + \rho_2 t + \sqrt{\rho_3^2 + \rho_4^3}e^{-\zeta_2\omega_{n,2}t}\sin\left(\omega_{r,2}t + \varphi_3\right) \tag{18}$$

where

$$\begin{cases} \rho_1 = -\Delta P_{d,\text{I}} - \rho_3 \;\; \rho_2 = \dfrac{\Delta P_{d,\text{sys}}\chi_3}{4H_{\text{sys}}^2} \\ \rho_3 = -\dfrac{2H_{\text{sys}}\omega_{n,2}\chi_1 - 2\zeta_2\Delta P_{d,\text{sys}}\chi_3}{4H_{\text{sys}}^2\omega_{n,2}} \\ \rho_4 = -\dfrac{2H_{\text{sys}}\zeta_2\omega_{n,2}\chi_1 + \Delta P_{d,\text{sys}}\left(1 - 2\zeta_2^2\right)\chi_3}{4H_{\text{sys}}^2\omega_{r,2}} \\ \varphi_3 = \tan^{-1}\dfrac{\rho_3}{\rho_4} \end{cases} \tag{19}$$

2) QUASI-STEADY STATE VALUE

When the dynamic process concludes, both the ITP and the RF cease to change, reaching quasi-steady-state values. At this point, the time constants of all dynamic components

no longer contribute delays, effectively becoming zero. Let this moment be denoted as t_∞, then it follows that $\dot{y}_{\mathrm{I}}(t_\infty)$ and $y_{\mathrm{II}}(t_\infty)$ are both constants, while $\ddot{y}_{\mathrm{I}}(t_\infty)$ and $\dot{y}_{\mathrm{II}}(t_\infty)$ are both zero. Substituting these values into (6), the analytical expressions for the quasi-steady-state values of the RF and the ITP can be derived as

$$\Delta f_{\mathrm{I}}^{\mathrm{qss}} = \Delta f_{\mathrm{II}}^{\mathrm{qss}} = \frac{\Delta P_{d,\mathrm{sys}}}{D_{\mathrm{sys}}^{\mathrm{qss}}} \tag{20}$$

$$\Delta P_t^{\mathrm{qss}} = -D_{\mathrm{I}}^{\mathrm{qss}} \Delta f_{\mathrm{I}}^{\mathrm{qss}} = -\frac{D_{\mathrm{I}}^{\mathrm{qss}} \Delta P_{d,\mathrm{sys}}}{D_{\mathrm{sys}}^{\mathrm{qss}}} \tag{21}$$

where

$$D^{\mathrm{qss}} = \frac{R}{DR + K_m} \tag{22}$$

As shown in Fig. 2, the peak value described by $\Delta P_{s,\mathrm{I}}^{(2)}(t)$ and the quasi-steady state value described by $\Delta P_t^{\mathrm{qss}}$ have extremely high accuracy when compared with the simulation results. Further validation will be performed in Section IV-A.

The obtained analytical expressions for the RF and the ITP, although simple in structure, are still transcendental equations formed by transcendental functions. Therefore, they cannot be analytically solved to obtain the required AFSIs. Section III will detail how to address this problem.

III. AFSIs FOR THE RF AND THE TIP

The proposed closed-form solutions for the two-machine frequency response model are multi-peak functions, which cannot be quickly solved for AFSIs using conventional methods. To obtain the required AFSIs, we need to divide different parts within the closed-form solution and weigh their importance in different stages of frequency dynamics. In this section, we partition the fast-varying part and the slow-varying part within the obtained analytical expressions. In the fast- varying part, certain terms may significantly impact transient frequency fluctuations, thus requiring focused attention and control over short periods. Conversely, in the slow- varying part, other terms may be crucial for the long-term stability of the system, influencing it over longer time scales. This yields AFSIs including nadir value, quasi-steady-state value, maximum rate value of RF, and peak value, quasi-steady-state value of ITP.

A. AFSI DEFINITIONS

Nadir value of RF: This refers to the nadir frequency reached within a region due to sudden events (such as load increase, generator failure, or other disturbances). It is mainly influenced by factors like rapid load changes, generator outages, large loads entering or leaving the system, and response speed of frequency regulation resources.

Quasi-steady-state value of RF: This indicates the frequency value that the system approaches but does not fully return to its original steady-state frequency after a disturbance. It is influenced by characteristics of frequency regulation control systems, dynamic properties of loads and generation, and system inertia.

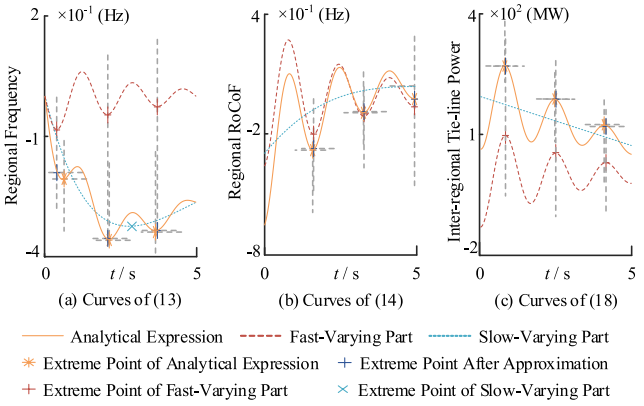

FIGURE 3. The analytical expression division and extreme point approximation.

Maximum rate value of RF: This measures the maximum rate at which frequency changes over time, typically in Hz/s. It is influenced by system inertia, instantaneous changes in load and generation, scheduling strategies, and control measures.

Peak value and quasi-steady-state value of ITP: These represent the maximum instantaneous power flow due to load changes or other disturbances between different regions connected by tie-lines. They are influenced by dynamic changes in inter-regional loads and generation, inter-regional power market transactions, system disturbances (such as faults, generator outages), tie-line capacities, and operational conditions.

B. FAST- AND SLOW-VARYING PARTS DIVISION

As shown in (13), (14) and (18), the analytical expressions all consist of functions with different angular frequencies (the angular frequencies of the constant terms and primary terms can be considered as 0). Depending on the magnitude of the angular frequencies, the expressions can be divided into the fast-varying part (large angular frequency) and the slow-varying part (small angular frequency).

Based on this method, the division results are as follows: the first terms of (13) and (14) are the slow-varying parts and the second terms are the fast-varying parts; the first two terms of (18) are the slow-varying parts and the third term is the fast-varying part. Fig. 3 illustrates their relationship.

As shown in Fig. 3, the extreme point moments of the analytical expressions are primarily determined by the fast-varying parts with minimal influence from the slow-varying parts. Exploiting this characteristic, the extreme point moments of the fast-varying parts can be used as an approximate substitute for the extreme point moments of the analytical expressions, and the approximate extreme points with high accuracy can be obtained. In the following, the AFSIs for the RF and the ITP are further deduced based on this approximation method.

C. NADIR VALUE OF THE RF

As shown in Fig. 3(a), influenced by the frequency spatial distribution characteristics, the nadir value of the RF shifts downward compared to that of the system frequency following a major disturbance. Simulation within a reasonable range of parameter values reveals that since the oscillation in the fast-varying part of the RF are damped and the oscillation amplitude is less than the deviation amplitude of the slow-varying part, the nadir value of the RF occurs in the fast-varying part before and after the extreme point moments of the slow-varying part.

Let the derivative of the slow-varying part in (13) be zero:

$$\Delta\dot{f}_{\mathrm{sv}}(t)=\alpha_1\omega_{n,1}e^{-\zeta_1\omega_{n,1}t}\sin\left(\omega_{r,1}t+\varphi_1\right)=0 \tag{23}$$

The nadir value moment of the slow-varying part can be derived as

$$t_{\mathrm{sv}}^{\mathrm{nadir}}=\frac{(2n^*+1)\,\pi-\varphi_1}{\omega_{r,1}} \tag{24}$$

where, the subscript sv stands for the slow part, the subscript fv stands for the FAST part, n^* is the first extreme point when $t_{\mathrm{sv}}^{\mathrm{nadir}}>0$:

$$n^*=\left\lceil\frac{\varphi_1-\pi}{2\pi}\right\rceil \tag{25}$$

Let the derivative of the fast-varying part in (13) be zero:

$$\begin{cases}\Delta\dot{f}_{\mathrm{fv,I}}(t)=-2H_{\mathrm{II}}\alpha_2\omega_{n,2}e^{-\varsigma_2\omega_{n,2}t}\sin\left(\omega_{r,2}t+\varphi_2\right)=0\\ \Delta\dot{f}_{\mathrm{fv,II}}(t)=2H_{\mathrm{I}}\alpha_2\omega_{n,2}e^{-\varsigma_2\omega_{n,2}t}\sin\left(\omega_{r,2}t+\varphi_2\right)=0\end{cases} \tag{26}$$

The extreme point moment of the fast-varying part in Region-I is the zero-point when $\sin\left(\omega_{r,2}t+\varphi_2\right)$ changes from positive to negative, and the nadir value moment of the fast-varying part in Region-II is the zero-point when $\sin\left(\omega_{r,2}t+\varphi_2\right)$ changes from negative to positive:

$$\begin{cases}t_{\mathrm{fv,I},\tau}^{\mathrm{Nadir}}=\frac{2\tau\pi-\varphi_3}{\omega_{r,2}},\\ t_{\mathrm{fv,II},\tau}^{\mathrm{Nadir}}=\frac{(2\tau+1)\pi-\varphi_3}{\omega_{r,2}},\end{cases}\quad\tau\in N \tag{27}$$

where, N stands for the positive integer.

Since the nadir value of the RF occurs before and after the nadir value of the slow-varying part:

$$\begin{cases}t_{\mathrm{sv}}^{\mathrm{nadir}}=t_{\mathrm{fv,I},\tau}^{\mathrm{nadir}}\Rightarrow\tau_1^*=\left\lceil\frac{t_{\mathrm{sv}}^{\mathrm{nadir}}\omega_{r,2}+\varphi_3}{2\pi}\right\rceil\\ t_{\mathrm{sv}}^{\mathrm{nadir}}=t_{\mathrm{fv,II},\tau}^{\mathrm{nadir}}\Rightarrow\tau_2^*=\left\lceil\frac{t_{\mathrm{sv}}^{\mathrm{nadir}}\omega_{r,2}+\varphi_3-1}{2\pi}\right\rceil\end{cases} \tag{28}$$

The nadir value of the RF can be derived as

$$\begin{cases}\Delta f_{\mathrm{I}}^{\mathrm{nadir}}=\min\left(\Delta f_{\mathrm{I}}\left(t_{\mathrm{fv,I},\tau}^{\mathrm{nadir}}\right)\right),\ \tau\in\left[\tau_1^*-1,\tau_1^*\right]\\ \Delta f_{\mathrm{II}}^{\mathrm{nadir}}=\min\left(\Delta f_{\mathrm{II}}\left(t_{\mathrm{fv,II},\tau}^{\mathrm{nadir}}\right)\right),\ \tau\in\left[\tau_2^*-1,\tau_2^*\right]\end{cases} \tag{29}$$

D. MAXIMUM RATE VALUE OF THE RF

The extreme points of (14) can be approximately obtained according to the pole time of the fast-varying parts. The derivative of the fast part in (3.45) - (3.46) is zero:

Let the derivative of the fast-varying part in (14) be zero:

$$\begin{cases}\Delta\ddot{f}_{\mathrm{fv,I}}(t)=-2H_{\mathrm{II}}\alpha_2\omega_{n,2}e^{-\zeta_2\omega_{n,2}t}\sin\left(\omega_{r,2}t+2\varphi_2\right)=0\\ \Delta\ddot{f}_{\mathrm{fv,II}}(t)=2H_{\mathrm{I}}\alpha_2\omega_{n,2}e^{-\zeta_2\omega_{n,2}t}\sin\left(\omega_{r,2}t+2\varphi_2\right)=0\end{cases} \tag{30}$$

The extreme point moments of the fast-varying part in Region-I and Region-II can be expressed as

$$t_{\mathrm{fv},\tau}^{\mathrm{RoCoF}}=\frac{\tau\pi-2\varphi_2}{\omega_{n,2}},\quad\tau\in N \tag{31}$$

Since both the fast-varying and slow-varying parts of (14) are damped, the maximum rate value can only occur at the initial moment or at the first extreme point moment. It is verified that the maximum rate value in the disturbed region occur at the initial moment and the maximum rate value in the non-disturbed region occur at the first extreme point moment when $t>0$:

$$\begin{cases}t_{\mathrm{max,I}}^{\mathrm{RoCoF}}=t_{\mathrm{FP},\tau^*}^{\mathrm{RoCoF}}=\frac{2\pi\tau^*-2\varphi_2}{\omega_{r,2}}\\ t_{\mathrm{max,II}}^{\mathrm{RoCoF}}=0\end{cases} \tag{32}$$

where

$$\tau^*=\left\lceil\frac{\varphi_2}{\pi}\right\rceil \tag{33}$$

The maximum rate value of the RF can be derived as

$$\begin{cases}\Delta\dot{f}_{\mathrm{max,I}}=\Delta\dot{f}_{\mathrm{I}}\left(t_{\mathrm{max,I}}^{\mathrm{RoCoF}}\right)\\ \Delta\dot{f}_{\mathrm{max,II}}=\Delta\dot{f}_{\mathrm{II}}(0)\end{cases} \tag{34}$$

E. PEAK VALUE OF THE ITP

Let the derivative of the fast-varying part in (18) be zero:

$$\begin{aligned}\Delta\dot{P}_{t,\mathrm{fv}}^{(2)}(t)=&-\omega_{n,2}\sqrt{\rho_3^2+\rho_4^3}e^{-\zeta_2\omega_{n,2}t}\\&\sin(\omega_{r,2}t+\varphi_2+\varphi_3)=0\end{aligned} \tag{35}$$

Therefore, the extreme point moments of the ITP is the zero-points of $\sin(\omega_{r,2}t+\varphi_2+\varphi_3)$. Since the oscillation power is also damped, the peak value of the ITP is the first swing peak, which is the first extreme point of (18):

$$t^{\mathrm{peak}}=\frac{\pi\tau^*-\varphi_2-\varphi_3}{\omega_{r,2}} \tag{36}$$

where

$$\tau^*=\left\lceil\frac{\varphi_2+\varphi_3}{\pi}\right\rceil \tag{37}$$

The peak value of the ITP can be derived as

$$\Delta P_t^{\mathrm{peak}}=\Delta P_{t,\mathrm{fv}}^{(2)}\left(t^{\mathrm{peak}}\right) \tag{38}$$

Besides, the quasi-steady-state values of the RF and the ITP are expressed as (20) and (21).

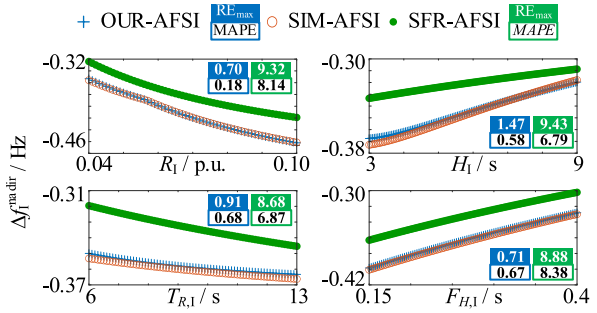

FIGURE 4. The Influence of parameter R, H, T_R, and F_H changes in the Region-I on the nadir value of the RF in the Region-I.

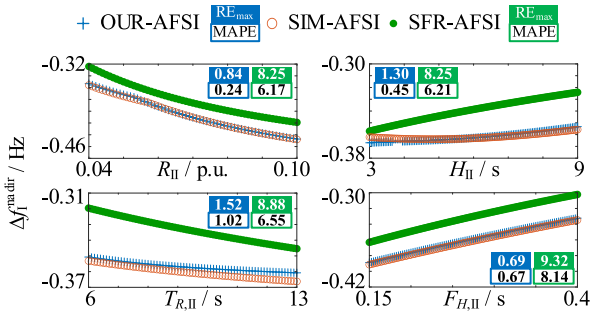

FIGURE 5. The Influence of parameter R, H, T_R, and F_H changes in the Region-II on the nadir value of the RF in the Region-I.

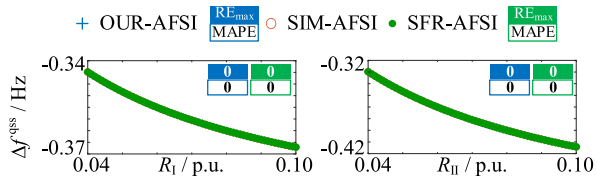

FIGURE 6. The Influence of parameter R changes on the quasi-steady-state value of the RF.

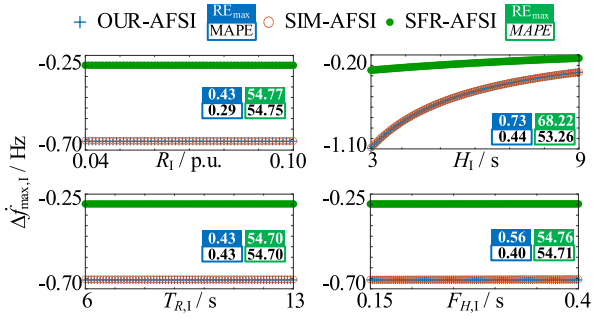

FIGURE 7. The Influence of parameter R, H, T_R, and F_H changes in the Region-I on the maximum rate value of the RF in the Region-I.

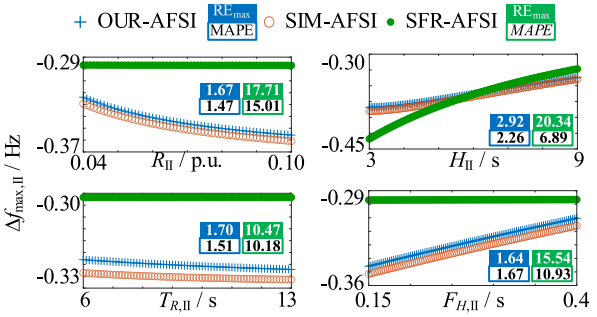

FIGURE 8. The Influence of parameter R, H, T_R, and F_H changes in the Region-II on the maximum rate value of the RF in the Region-I.

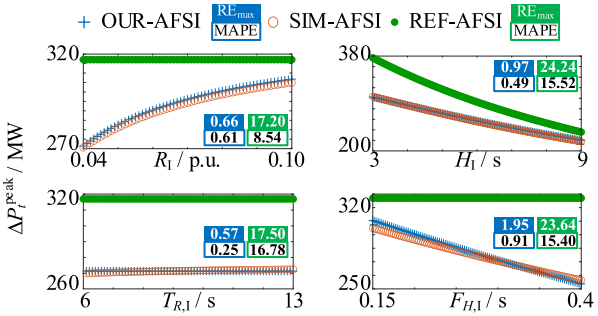

FIGURE 9. The Influence of parameter R, H, T_R, and F_H changes in the Region-I on the peak value of the ITP.

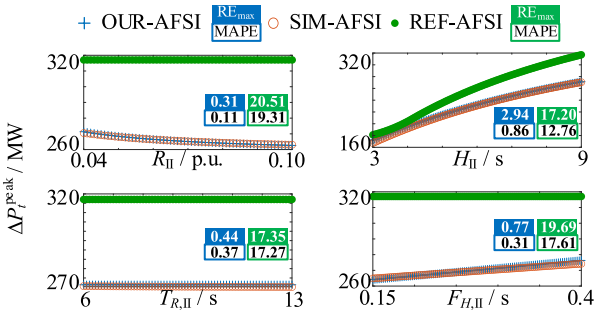

FIGURE 10. The Influence of parameter R, H, T_R, and F_H changes in the Region-II on the peak value of the ITP.

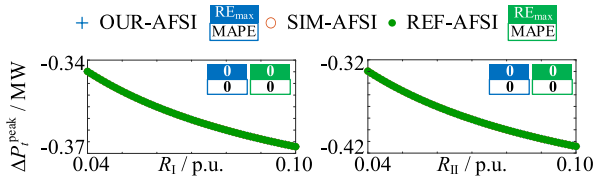

FIGURE 11. The Influence of parameter R changes on the quasi-steady-state of the ITP.

IV. CASE STUDIES

A. SCENARIO SETTING

To conduct a broader accuracy verification and parameter sensitivity analysis of the obtained AFSIs, this section presents case studies based on the IEEE 2-region 4-machine system. The system structure and dynamic parameters are detailed in Appendix A. A disturbance is introduced into the system at t=0s, where a sudden increase of 300MW load occurs at Bus-7 in Region-I, representing 7.5% of the system capacity. The error comparison and sensitivity analysis of the AFSIs are conducted using control variable method (changing the dynamic parameters of Region-I or Region-II). It's worth noting that since the normalized values of parameters based on system capacity fall within the same range regardless of the system's scale, conducting parameter sensitivity analysis based on this range ensures the universality of the conclusions.

The accuracy verification and parameter sensitivity analysis is conducted through various methods, the comparisons are shown in Fig. 4-Fig. 11. In these figures, SIM-AFSI

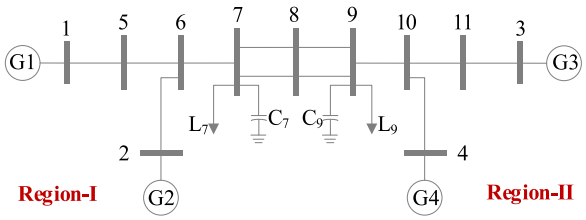

FIGURE 12. The IEEE 2-region 4-machine system.

TABLE 1. The power data of generator, load and capacitor.

Power	Generator				Load		Capacitor	
	G_1	G_2	G_3	G_4	L_7	L_9	C_7	C_9
P/MW	400	625	550	450	695	1259	-	-
Q/Mvar	105	208	134	129	72	72	144	252

TABLE 2. The parameters and their typical value range of the low-order governor model.

Parameter	G_1	G_2	G_3	G_4	Typical value range
H_i	5	5	9	9	3~9
$F_{H,i}$	0.3	0.3	0.3	0.3	0.15~0.40
$T_{R,i}$	7	7	7	7	6~14
R_i	0.04	0.04	0.04	0.04	0.04~0.10

represents the benchmark results solved by the high-order simulation model, OUR-AFSI represents the results solved by the two-region model proposed in this paper, SFR-AFSI represents the results solved by the uniform-frequency model [10], REF-AFSI represents the results of peak and steady-state values solved by [26] and [27] respectively, RE_{max} represents the maximum relative error, and MAPE represents the Mean Absolute Percentage Error.

B. ACCURACY VERIFICATION

As shown in Fig. 4 - Fig. 11, compared with the simulation results, the RE_{max} and MAPE of the proposed AFSIs are very close, and most of the RE_{max} and MAPE are less than 1 %, and the maximum RE_{max} and MAPE are 2.92% and 2.26%, respectively. Therefore, the proposed AFSIs show extremely high accuracy and good robustness.

Further comparison with the SFR-AFSI and the REF-AFSI shows that, in addition to the quasi-steady-state values of the RF and the ITP, the accuracy of the proposed AFSIs is greatly improved by at least 67% and up to 99.47%. For the quasi-steady-state values, the results of each method are the same, and it can be seen that the quasi-steady-state values are not affected by the frequency spatial distribution characteristics.

C. PARAMETER SENSITIVITY ANALYSIS

As shown in Fig. 4 - Fig. 6, the influence of regional parameter changes on the nadir value and the quasi-steady-state value of the RF is the same. Among them, the nadir value is negatively correlated with R and T_R, and positively correlated with H and F_H, the quasi-steady-state value is negatively correlated with R and has nothing to do with the other parameters. Therefore, when it is necessary to increase the nadir value and the quasi-steady-state value of any region, priority should be given to increasing the primary frequency regulation resources with lower cost, without paying attention to the region where the resources are located.

As shown in Fig. 7 - Fig. 8, the influence of regional parameter changes on the maximum rate value of the RF in the two regions is not exactly the same, but not the opposite. Among them, the maximum rate value in the disturbed region is only positively correlated with H within this region, and has nothing to do with the other parameters, the maximum rate value in the non-disturbed region is positively correlated with H and F_H, negatively correlated with R, and is more affected by the parameter changes within this region. Therefore, when it is necessary to increase the maximum rate value of any region, priority should be given to the primary frequency regulation resources with lower cost within the region.

As shown in Fig. 9 - Fig. 11, the influence of regional parameter changes on the peak value and quasi-steady-state value of the ITP is opposite. Among them, the peak value is positively correlated with R and negatively correlated with H and F_H of the disturbed region, while in the non-disturbed region, the correlation is opposite. The quasi-steady state value is positively correlated with R of the disturbed region and negatively correlated with R of the non-disturbed region.

Therefore, the AFSIs of the ITP depends on the comparative primary frequency regulation capabilities of the two regions. The stronger the capability of the disturbed region, the smaller the AFSIs of the ITP. While enhancing the primary frequency regulation capability, it is crucial to ensure coordination between the capabilities of the two regions. Considering the more severe situation in the disturbed region, priority should be given to increasing the primary frequency regulation capability of the disturbed region when the AFSIs of the ITP exceeds the limit.

V. CONCLUSION

This paper focuses on the two-region interconnected power system and derives the analytical expressions for the RF and the ITP based on the low-order frequency response model. By dividing the fast-varying part and the slow-varying part of the obtained analytical expressions, AFSIs for the RF and the ITP are further derived.

The obtained AFSIs can accurately describe the frequency security situation following a major disturbance, including nadir value, quasi-steady-state value, maximum rate value of the RF, and peak value, quasi-steady-state value of the ITP. These indicators can provide formulas for analytical analysis and rapid computation.

Based on the research in this paper, further studies can be conducted on frequency situation awareness, frequency

TABLE 3. The parameters of generator, exciter and governor in the high-order simulation model.

Model	Parameter							
GENROU Generator	T'_{d0}	T''_{d0}	T'_{q0}	T''_{q0}	D	X_d	X_q	X'_d
	8	0.03	0.4	0.05	0	1.8	1.7	0.3
	X'_q	X''_d=X''_q	X_1	S(1.0)	S(2.0)	-	-	-
	0.55	0.25	0.2	0.0392	0.2672	-	-	-
ESDC1A Exciter	T_R	K_A	T_A	T_B	T_C	VR_{max}	VR_{min}	K_E
	0.05	20	0.055	0	0	5	-3	1
	T_E	T_F	T_F	*0.Switch*	*E1*	*SE(E1)*	*E2*	*SE(E2)*
	0.36	0.125	1.8	0	3	0.1	4	0.3
IEEEG1 Governor	R	T_3	T_4	T_5	T_6	U_0	U_C	P_{max}
	0.04	0.1	0.1	7	0.3	0.3	-0.3	1
	P_{min}	K_1	K_3	K_5	T_1=T_2=T_7		K_2=K_4=K_6=K_7	
	0	0.3	0.4	0.3	0		0	

emergency control, and frequency safety constrained unit commitment in two- region interconnected power systems.

Due to inherent limitations of analytical methods, the accuracy of AFSIs derived in this paper is relatively lower compared to simulation methods. Therefore, they are typically suitable for scenarios that prioritize high computational speed.

Therefore, the AFSIs proposed in this paper can serve as a basis for studies such as frequency state awareness, frequency emergency control, and optimal unit commitment under frequency safety constraints. Building upon this study, our future research will delve deeper into these areas.

.

APPENDIX A SYSTEM STRUCTURE AND DYNAMIC PARAMETERS

The IEEE 2-region 4-machine system is shown in Fig. 12. The power data of generator, load and capacitor are shown in Table 1. The parameters and their typical value range of the low-order governor model are shown in Table 2. The parameters of generator, exciter and governor in the high-order simulation model are shown in Table 3.

REFERENCES

[1] W. Wang, Z. Wang, X. Liu, W. Li, Q. Li, Y. Zhang, Q. Chen, S. Guo, and Z. Xu, "Frequency response mode prediction of power system after large disturbances based on deep belief neural network," *IEEE Access*, vol. 11, pp. 113653–113666, 2023.

[2] X. Cai, N. Zhang, E. Du, Z. An, N. Wei, and C. Kang, "Low inertia power system planning considering frequency quality under high penetration of renewable energy," *IEEE Trans. Power Syst.*, vol. 39, no. 2, pp. 4537–4548, Mar. 2024.

[3] Q. Hong, M. A. U. Khan, C. Henderson, A. Egea-Àlvarez, D. Tzelepis, and C. Booth, "Addressing frequency control challenges in future low-inertia power systems: A great Britain perspective," *Engineering*, vol. 7, no. 8, pp. 1057–1063, Aug. 2021.

[4] B. Wang, S. Zhu, G. Cai, D. Yang, Z. Chen, J. Ma, and Z. Sun, "Sparse measurement-based modelling low-order dynamics for primary frequency regulation," *IEEE Trans. Power Syst.*, vol. 39, no. 1, pp. 1–11, Jan. 2023.

[5] X. Li, Z. Wang, Y. Liu, Z. Wang, L. Zhu, L. Guo, C. Zhang, J. Zhu, and C. Wang, "The largest estimated domain of attraction and its applications for transient stability analysis of PLL synchronization in weak-grid-connected VSCs," *IEEE Trans. Power Syst.*, vol. 38, no. 5, pp. 1–14, Sep. 2022.

[6] G. Zhao, L. Ding, and M. Liu, "Characterization of frequency spatial distribution of power system under disturbance scenario," in *Proc. IEEE Int. Conf. Adv. Power Syst. Autom. Protection (APAP)*, Oct. 2023, pp. 578–583.

[7] Y. Zhang, X. Shi, H. Zhang, Y. Cao, and V. Terzija, "Review on deep learning applications in frequency analysis and control of modern power system," *Int. J. Electr. Power Energy Syst.*, vol. 136, Mar. 2022, Art. no. 107744.

[8] L. Xu, L. Li, M. Wang, X. Wang, Y. Li, W. Li, and K. Zhou, "Online prediction method for power system frequency response analysis based on swarm intelligence fusion model," *IEEE Access*, vol. 11, pp. 13519–13532, 2023.

[9] O. Shariati, M. R. Aghamohammadi, B. Potter, and M. Mirheydar, "A novel approach to extended system frequency response model for complex power systems (ESFR)," *IEEE Access*, vol. 11, pp. 60777–60791, 2023.

[10] P. M. Anderson and M. Mirheydar, "A low-order system frequency response model," *IEEE Trans. Power Syst.*, vol. 5, no. 3, pp. 720–729, Aug. 1990.

[11] T. Wang, S. Ma, S. Wang, W. Hou, J. Gao, J. Guo, and X. Zhou, "Modal analysis-based analytical method for frequency estimation during inertia response stage of power systems," *IEEE J. Emerg. Sel. Topics Circuits Syst.*, vol. 13, no. 3, pp. 692–701, Sep. 2023.

[12] M. Paturet, U. Markovic, S. Delikaraoglou, E. Vrettos, P. Aristidou, and G. Hug, "Stochastic unit commitment in low-inertia grids," *IEEE Trans. Power Syst.*, vol. 35, no. 5, pp. 3448–3458, Sep. 2020.

[13] J. Zhang, Y. Wang, H. Li, G. Zhou, B. Li, L. Wang, and K. Li, "SFR modeling for hybrid power systems based on deep transfer learning," *IEEE Trans. Ind. Informat.*, vol. 20, no. 1, pp. 399–410, Jan. 2024.

[14] U. Markovic, Z. Chu, P. Aristidou, and G. Hug, "LQR-based adaptive virtual synchronous machine for power systems with high inverter penetration," *IEEE Trans. Sustain. Energy*, vol. 10, no. 3, pp. 1501–1512, Jul. 2019.

[15] D. Lekshmi J, Z. H. Rather, and B. C. Pal, "Online estimation of disturbance size and frequency nadir prediction in renewable energy integrated power systems," *IEEE Trans. Power Syst.*, vol. 39, no. 1, pp. 1–11, Jan. 2023.

[16] H. Zhang, K. Wei, Y. Wei, and H. Zhu, "Emergency power control strategy of HVDC FLC based on modified SFR model in islanded HVDC sending system," *Int. J. Electr. Power Energy Syst.*, vol. 142, Nov. 2022, Art. no. 108314.
[17] J. Huang, Z. Yang, J. Yu, J. Liu, Y. Xu, and X. Wang, "Optimization for DFIG fast frequency response with small-signal stability constraint," *IEEE Trans. Energy Convers.*, vol. 36, no. 3, pp. 2452–2462, Sep. 2021.
[18] Y. Shen, W. Wu, B. Wang, Y. Yang, and Y. Lin, "Data-driven convexification for frequency nadir constraint of unit commitment," *J. Modern Power Syst. Clean Energy*, vol. 11, no. 5, pp. 1–7, 2022.
[19] X. Fu, J. Song, F. Yue, H. Li, G. Li, and H. Liu, "An extended SFR model of offshore wind farm integrated by VSC-HVDC for frequency support," in *Proc. IEEE/IAS Ind. Commercial Power Syst. Asia*, 2023, pp. 1286–1291.
[20] L. Liu, W. Li, Y. Ba, J. Shen, C. Jin, and K. Wen, "An analytical model for frequency nadir prediction following a major disturbance," *IEEE Trans. Power Syst.*, vol. 35, no. 4, pp. 2527–2536, Jul. 2020.
[21] Z. Li, J. Liu, S. Liu, Z. Guo, Z. Zhang, J. Rong, and M. Zhou, "Quantifying spatial-related inertia value for high share of wind power integration," *IEEE Access*, vol. 10, pp. 113100–113112, 2022.
[22] V. Van Huynh, P. Thanh Tran, C. Si Thien Dong, B. Dinh Hoang, and O. Kaynak, "Sliding surface design for sliding mode load frequency control of multiarea multisource power system," *IEEE Trans. Ind. Informat.*, vol. 20, no. 5, pp. 7797–7809, May 2024.
[23] C. You, Y. Zhao, S. Hou, Y. Zhang, and Y. Lv, "Research on centre of inertia based frequency sampling and system frequency distribution characteristics," *IEEE Access*, vol. 12, pp. 71371–71378, 2024.
[24] P. Rabbanifar and N. Amjady, "Frequency-constrained unit-commitment using analytical solutions for system frequency responses considering generator contingencies," *IET Gener., Transmiss. Distrib.*, vol. 14, no. 17, pp. 3548–3560, Sep. 2020.
[25] J. Shen, W. Li, L. Liu, C. Jin, K. Wen, and X. Wang, "Frequency response model and its closed-form solution of two-machine equivalent power system," *IEEE Trans. Power Syst.*, vol. 36, no. 3, pp. 2162–2173, May 2021.
[26] X. Wang, W. Li, J. Shen, S. Zhao, and Q. Zhang, "A three-machine equivalent system frequency response model and its closed-form solution," *Int. J. Electr. Power Energy Syst.*, vol. 142, Nov. 2022, Art. no. 108344.
[27] Y. Tang, D. Sun, J. Yi, and W. Lin, "AC tie-line power fluctuation mechanism and peak value calculation for two-area interconnected power systems," *Chin. Soc. Elect. Eng.*, vol. 30, no. 19, pp. 1–6, Jul. 2010.
[28] P. Rabbanifar and S. Jadid, "Stochastic multi-objective tie-line power flow and frequency control in market clearing of multi-area electricity markets considering power system security," *IET Gener., Transmiss. Distribution*, vol. 8, no. 12, pp. 1960–1978, Dec. 2014.
[29] J. Tu, L. Yang, Y. Huang, and H. Zhao, "Mechanism and peak value calculation of AC tie-line power swing caused by DC blocking," *Electr. Power Autom. Equip.*, vol. 33, no. 1, pp. 12–17, Jan. 2013.
[30] D. A. L. Roca, P. Mercado, and G. Suvire, "System frequency response model considering the influence of power system stabilizers," *IEEE Latin Amer. Trans.*, vol. 20, no. 6, pp. 912–920, Jun. 2022.
[31] A. Perdana, "Dynamic models of wind turbines," Ph.D. dissertation, Dept. Energy Environ., Chalmers Univ. Technol., Gothenburg, Sweden, 2008.

QIANG ZHANG was born in 1982. He received the M.S. degree in electrical engineering from Xi'an Jiaotong University (XJTU), Xi'an, China, in 2008. He is mainly responsible for the safety and stability analysis of power system with the State Grid Liaoning Electric Power Research Institute. His research interests include power system stability and control and new energy measurement modeling.

XINWEI LI was born in 1993. She received the Master of Science degree in engineering from North China Electric Power University (NCEPU), Beijing, China, in 2019. She is currently with the Electric Power Research Institute, State Grid Liaoning Provincial Electric Power Company Ltd. Her research interests include power system stability analysis, risk assessment, and control of power grid.

GUORONG LAN (Graduate Student Member, IEEE) was born in 2001. He received the B.S. degree in electrical engineering and automation from Dalian Maritime University, Dalian, China, in 2023. He is currently pursuing the master's degree with the School of Electrical Engineering, Dalian University of Technology, Dalian. His research interests include the modeling, analysis, and simulation of frequency response in power systems.

XIANGXU WANG (Graduate Student Member, IEEE) was born in 1997. He received the B.S. degree in electrical engineering from Dalian University of Technology (DUT), Dalian, China, in 2019, where he is currently pursuing the Ph.D. degree with the School of Electrical Engineering. His research interests include the modeling, analysis, and simulation of frequency response in power systems.

JIAKAI SHEN was born in 1991. He received the Ph.D. degree in power system and its automation from Dalian University of Technology, Dalian, China, in 2022. He is currently with China Electric Power Research Institute Company Ltd. His research interests include the modeling, simulation, analysis, and control of primary frequency response in power systems.

HUI ZENG was born in 1984. He received the master's degree in energy systems and in engineering and technical management from The University of New South Wales, Sydney Australia, in 2011. He is currently pursuing the Ph.D. degree with the School of Electrical Engineering, Dalian University of Technology. His research interests include modeling, analysis, and simulation of inertia in power systems.

PENG YUAN was born in 1994. He received the M.Eng. degree in electrical engineering from Dalian University of Technology (DUT), Dalian, China, in 2019. His current research interests include power market analysis, power system analysis, and optimal scheduling, with a focus on spot markets and ancillary services markets.

XIAOHENG ZHANG was born in 1994. She received the M.S. degree in electrical engineering from Northeast University (NEU), Liaoning, China, in 2020. She is mainly responsible for the safety and stability analysis of power system with the State Grid Liaoning Electric Power Research Institute. Her research interests include power system analysis, power system stability, new energy measurement modeling.

WEIDONG LI (Member, IEEE) received the B.S. degree in electrical engineering from Xi'an Jiaotong University, Xi'an, China, in 1985, the M.S. degree in electrical engineering from Northeast Electric Power University, Jilin, China, in 1988, and the Ph.D. degree in electrical engineering Harbin Institute of Technology, Harbin, China, in 1997. He is currently a Professor in electrical engineering with Dalian University of Technology, Dalian, China, where he was the Dean of the School of Electrical Engineering, from 2011 to 2016. His research interests include power system automation, with a recent focus on frequency stability analysis and control of new power systems.